



ISSN NO. 2320-5407

Journal homepage: <http://www.journalijar.com>

INTERNATIONAL JOURNAL  
OF ADVANCED RESEARCH

## RESEARCH ARTICLE

### Reinforced sisal fiber with aluminum nitrate composites

Asif Jehan<sup>1</sup>, Dr. Shirish Joshi<sup>2</sup> and Dr. M.N. Bapat<sup>3</sup>

1. 2. Motilal vigyan mahavidhalya Bhopal (M.P.) India

3. regional institute of education Bhopal (M.P.) India

#### Manuscript Info

##### Manuscript History:

Received: 18 March 2015  
Final Accepted: 22 April 2015  
Published Online: May 2015

##### Key words:

Al<sub>2</sub>O<sub>3</sub>, sintering method, XRD,  
TEM, SEM, FTIR and ε

##### \*Corresponding Author

Asif Jehan

#### Abstract

Aluminum oxide synthesized through annealing route. The present research work deals with aluminum composite prepared using chemical reactions. Aluminum nitrates and ammonium chloride doped with sisal fiber has been prepared. The structural behavior of aluminum oxide was studied in XRD, SEM, TEM, FTIR and dielectric measurement (ε). This behavior showed aluminum nature of the sample.

Copy Right, IJAR, 2015,. All rights reserved

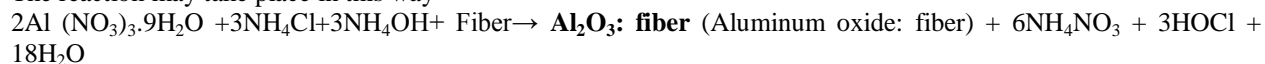
## INTRODUCTION

Aluminum oxides including alumina (Al<sub>2</sub>O<sub>3</sub>) and boehmite (AlOOH) get large attention because those are widely used in many applications, for example, adsorbents for removal of HF and water, fabrication of porous ceramics, 3,4 and composite materials for organic/inorganic hybrid coatings [1-6]. A new class of nano-and submicron-sized wire, tube, mats, and belts made to attract a very large research interest in the last few years [7-12]. In this note, we report the physical properties of aluminum oxide submicron-rings (AO-SMRs) obtained by using electro spinning technique. Alumina (Al<sub>2</sub>O<sub>3</sub>-corundum structure) is an extremely useful ceramic in many existing and emerging technologies. These include bio-medical implants, the production of which often involves co-firing with metals. High density in alumina components is normally achieved by sintering compacted alumina powder above 1700°C [13, 14]. However, many of the metals used in the bio-medical industry have melting points close to or below the generally required sintering temperature of alumina (such as Ti (1610°C) and stainless steel (~1400°C)). One list of biocompatible metals is given in Merrill et al. [15]. In addition, a reduced alumina sintering temperature would have other advantages. These include reduced processing costs and finer sintered grain sizes. Various methods have been employed to combat the generally high temperatures required to sinter alumina powder into useful ceramic monoliths. One such method is the introduction of dopants in the pre-fired alumina. Minor additions of oxides such as MnO<sub>2</sub> and/or TiO<sub>2</sub> are known to allow dense alumina to be synthesized at temperatures as low as 1400°C [13]. A combination of several dopants has seen the greatest decreases in densification temperatures [16, 17]. The decrease in densification temperature may be due to the formation of a grain boundary film of liquid eutectic, or defects in the structure which increases bulk diffusion rates [18]. This has been achieved using some specialized techniques, including sol-gel processing; the in-flight oxidation of nano-sized alumina using a plasma reactor, solution based combustion synthesis, and pulsed wire evaporation [19-22]. These processes, while interesting, may have limited applicability on an industrial scale due to the small quantities of powder produced, the availability and cost of such specialized equipment, and large operating costs. Grain size reduction can also be achieved using mechanical grinding processes. High energy mechanical milling has been used to produce nano meter sized particles in many materials including alumina [23].

### 1. Process

Aluminum Nitrate ( $\text{Al}(\text{NO}_3)_3 \cdot 9\text{H}_2\text{O}$ ) and ammonium chloride ( $\text{NH}_4\text{Cl}$ ) was taken in the ratio 10:4 in 500 ml of distilled water. The mixture was stirred till a homogenous solution was obtained. In this mixture 10g of processed sisal fiber was added and then 1:1 solution of  $\text{NH}_4\text{OH}$  (liquid ammonia) was added to it and left the solution for one hour. Again the mixture thus obtained was dried and then annealed in muffle furnace at  $1000^\circ\text{C}$  and kept it at that temperature for different time duration sample 1 (SP1) for 15 min, sample 2 (SP2) for 30 min and sample 3 (SP3) for 45 min.

The reaction may take place in this way



When aluminum nitrate reacts with ammonium chloride and ammonium hydroxide along with sisal fiber at  $1000^\circ\text{C}$  aluminum oxide is formed which is confirmed through XRD analysis and other by products like  $6\text{NH}_4\text{NO}_3$  Ammonium nitrate and HOCl (hypochlorous acid) decomposed at such high temperature and only aluminum oxide is left.

## 2. Result and discussion

### 3.1 X-Ray diffraction

XRD analysis shows that treated sisal fibre composites are crystalline in nature and shows the traces of  $\text{Al}_2\text{O}_3$ : fibre. The amorphous state of the sisal fiber composite was verified by XRD. The x-ray diffraction patterns of SP1  $\text{Al}_2\text{O}_3$  doped with sisal fiber shown in fig 1. The main peaks for  $\text{Al}_2\text{O}_3$  are observed at  $2\theta=10.789$  ( $d=8.19980 \text{ \AA}$ ),  $2\theta=45.574$  ( $d=1.98885 \text{ \AA}$ ),  $2\theta=66.865$  ( $d=1.39813 \text{ \AA}$ ) and  $2\theta=37.324$  ( $d=2.40728 \text{ \AA}$ ) corresponding to (416), (132), (164), and (132) reflections.

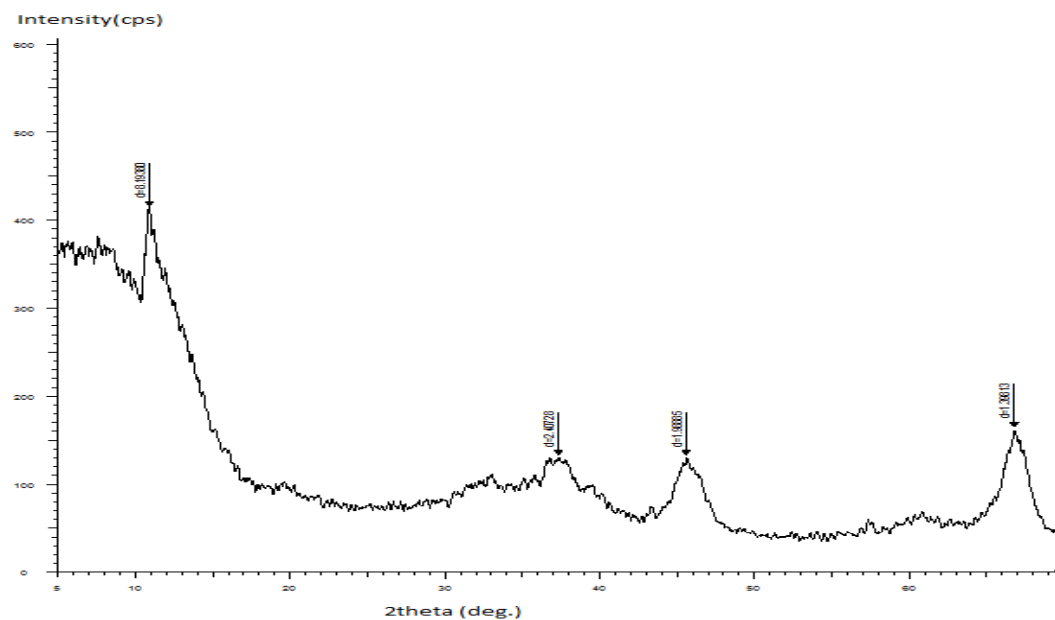


Fig 1

The peaks present in  $\text{Al}_2\text{O}_3$  were also observed in the composition of sisal fiber with  $\text{Al}_2\text{O}_3$  which indicates the presence of Alumina particle. The entire pattern indicates about the small dimensions of the Aluminum oxide particles. The changes in peaks occur due to the presence of composition of sisal fiber [24]. The x-ray diffraction patterns of SP2  $\text{Al}_2\text{O}_3$  doped with sisal fiber shown in fig 2. The main peaks for  $\text{Al}_2\text{O}_3$  are observed at  $2\theta=25.285$  ( $d=3.5194 \text{ \AA}$ ),  $2\theta=29.540$  ( $d=3.0214 \text{ \AA}$ ),  $2\theta=34.845$  ( $d=2.5726 \text{ \AA}$ ),  $2\theta=37.460$  ( $d=2.3988 \text{ \AA}$ ),  $2\theta=43.025$  ( $d=2.1006 \text{ \AA}$ ),  $2\theta=52.200$  ( $d=1.7509 \text{ \AA}$ ),  $2\theta=57.180$  ( $d=1.6097 \text{ \AA}$ ),  $2\theta=66.170$  ( $d=1.4111 \text{ \AA}$ ),  $2\theta=67.845$  ( $d=1.3803 \text{ \AA}$ ),  $2\theta=76.520$  ( $d=1.2439 \text{ \AA}$ ) corresponding to (914), (269), (1629), (930), (1980), (888), (1725), (936), (1161) and (289) reflections.

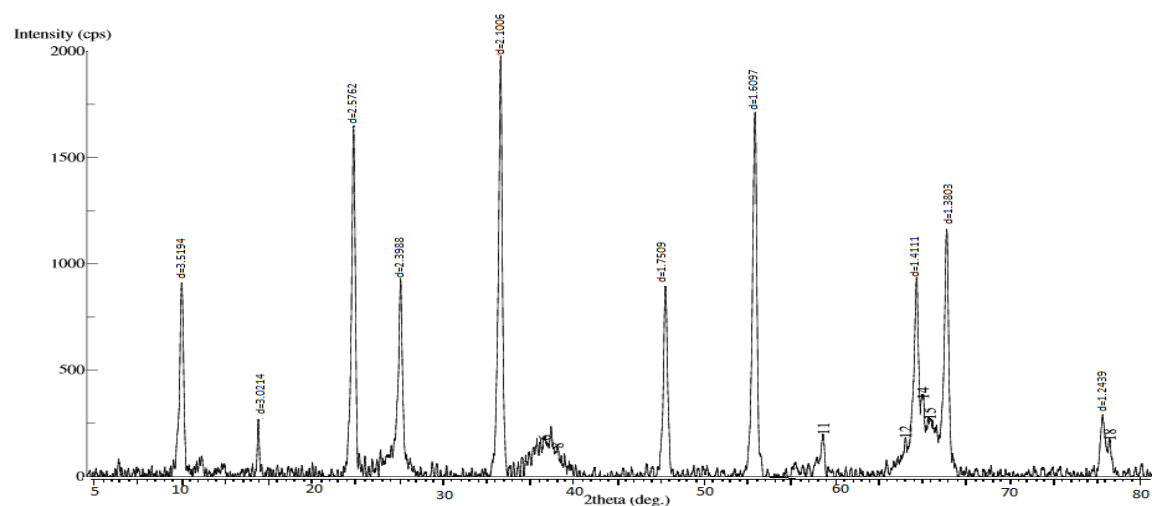


Fig 2

These radical cations through the coupling reaction lead to the ion of stable electrically conducting natural fiber. Reaction with the natural fiber generated by an internal redox reaction, which causes the reorganization of electronic structure to give the +ve and -ve nature of a radical is linked to its difference in reactivity towards lignin and cellulose/hemicelluloses [25]. The x-ray diffraction patterns of SP3  $\text{Al}_2\text{O}_3$  doped with sisal fiber shown in fig 3. The main peaks for  $\text{Al}_2\text{O}_3$  are observed at  $2\theta=25.330$  ( $d=3.5133 \text{ \AA}$ ),  $2\theta=34.890$  ( $d=2.5694 \text{ \AA}$ ),  $2\theta=37.505$  ( $d=2.3960 \text{ \AA}$ ),  $2\theta=43.075$  ( $d=2.0982 \text{ \AA}$ ),  $2\theta=52.265$  ( $d=1.7489 \text{ \AA}$ ),  $2\theta=57.225$  ( $d=1.6085 \text{ \AA}$ ),  $2\theta=61.000$  ( $d=1.5177 \text{ \AA}$ ),  $2\theta=66.220$  ( $d=1.4101 \text{ \AA}$ ),  $2\theta=67.895$  ( $d=1.3794 \text{ \AA}$ ),  $2\theta=76.585$  ( $d=1.2430 \text{ \AA}$ ) corresponding to (2296), (3887), (1915), (4481), (2112), (4019), (333), (1707), (2564) and (664) reflections.

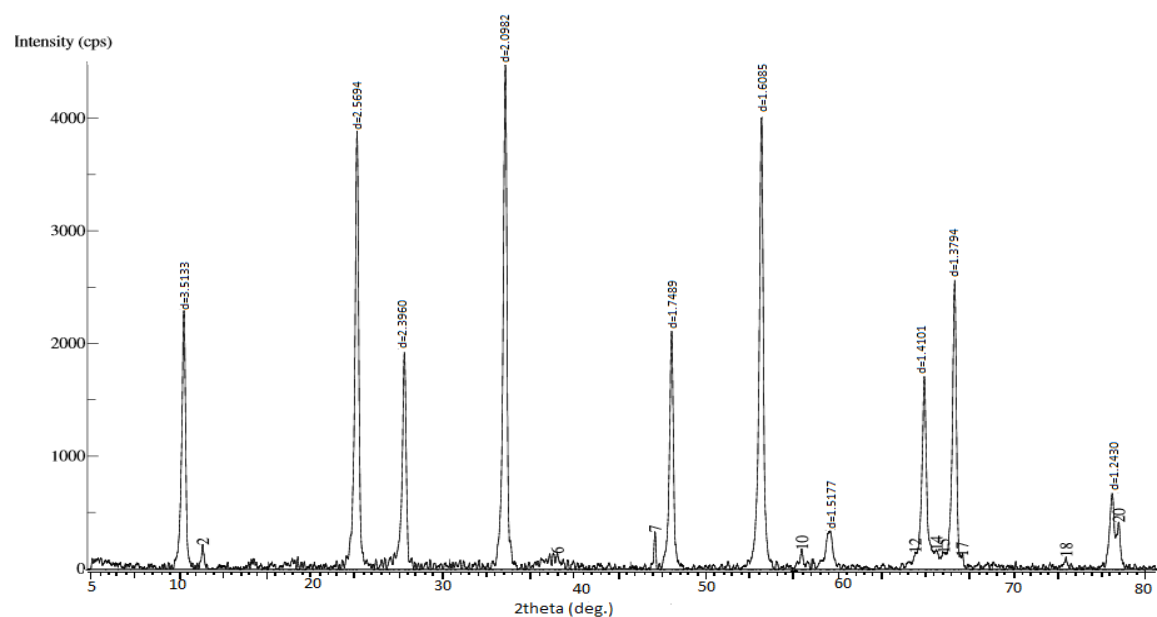


Fig 3

Natural sisal fiber consists of proton  $\text{H}^+$  molecule in its composition and deprotonation process is also occurred in natural fiber. Deprotonation is the removal of a proton ( $\text{H}^+$ ) from a molecule. Deprotonation of the radical cation is a major pathway and the proton removal decreases positive charge in the molecule and an increases negative charge.

Deprotonation usually occurs from the donation of electrons or acceptance of the proton using a base, which forms its conjugate acid [26].

Name	Symbol	Classification	A	B
Cellulose	$C_6H_{10}O_5$	C-H Deprotonation	C	H
Hemicelluloses	$C_5H_{10}O_5$	C-H Deprotonation	C	H
Lignin	$C_{13}H_{34}O_{11}$	C-H Deprotonation	C	H

Some unknown peaks are present in the XRD graphs. Hence other crystalline phases such as various types of hydrated aluminum nitrate, ammonium chloride, sisal fiber or other impurities; might have been present in sample. Aluminum oxide cannot be produced at relatively very low temperature; therefore, it is not possible for nitrate ions to decompose. So that it's calcinated on high temperature at  $1000^\circ\text{C}$  the 2 $\theta$  peaks (or miller indices) which indicates that  $Al_2O_3$  was present. As the time increased from 15 min (SP1), 30 min (SP2) and 45 min (SP3), the intensity of  $Al_2O_3$  phase peaks of SP2 increased as compare to SP1 and peaks of SP3 decreased as compare to SP2. The XRD results do not show that the sample was hydrated salt with other impurities. Therefore water molecules and impurities already removed at this temperature. After being calcinated at  $1000^\circ\text{C}$  the sample lost its crystalline structure and small amorphous humps appeared at  $2\theta = 5-8^\circ, 32-38^\circ$  and  $57-62^\circ$  for SP1;  $2\theta = 11-13^\circ, 36-41^\circ$  and  $55-59^\circ$  for SP2;  $2\theta = 11-12^\circ, 35-40^\circ$  and  $55-57^\circ$  for SP3. These humps are due to the interference of XRD signals of aluminum oxide. At this temperature  $Al_2O_3$  phases lose their bonding and appear highly amorphous in nature its intensity of humps increased. These results indicate that at this temperature the aluminum oxide particles in several crystallize aluminum oxide. These finding was confirmed by referring to the XRD data base reference data base (KSD collection code 025778). The crystal system of the structure was rhombohedral and had a density of  $4.02\text{cm}^{-3}$ . The XRD peaks of SP2 and SP3 indicated the presence of  $\alpha$ -aluminum oxide were at  $2\theta$  (miller indices) for SP2= 25.285, 29.540, 34.845, 43.025, 52.200, 57.180, 66.170, 67.845, 76.520 and for SP3= 25.330, 34.890, 37.505, 43.075, 52.265, 57.225, 61.000, 66.220, 67.895, 76.585. Some of the reading has been verified due to impurities. The intensity of XRD peaks increased, indicating that more  $\alpha$ -aluminum oxide crystals [27].

### 3.2 SEM

Figures 4, 5 & 6 show the scanning electron microscopy of sisal fiber treated with aluminum oxide composites which were fired at  $1000^\circ\text{C}$ . We can notice from the figures that there is change in the morphology of treated sisal fibre.

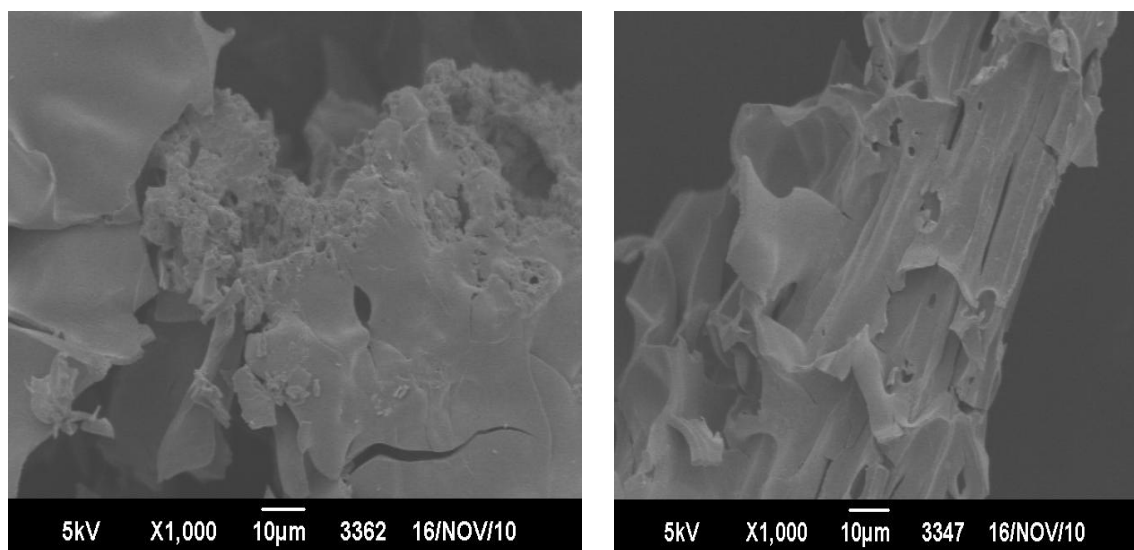


Fig 4 (a) and (b)

A change in the morphology and structure has been found after the treatment of sisal fibre which is confirmed by SEM technique. Figure 4, 5 & 6 shows the morphology of  $Al_2O_3$ . The variations in specular optical transmittance against wavelength for pure and doped Aluminum oxide.

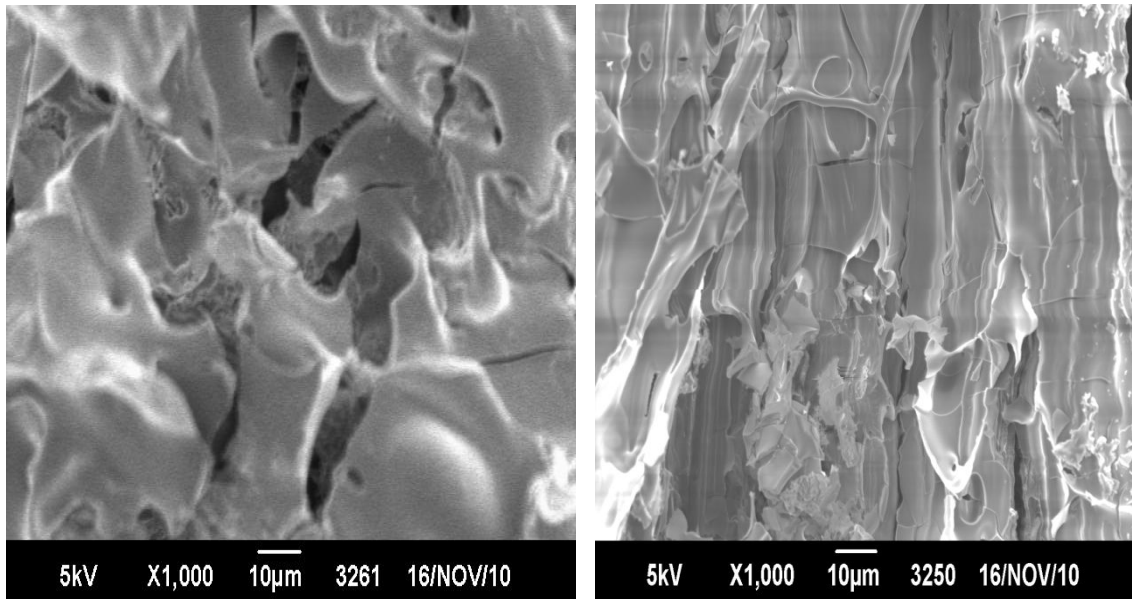


Fig 5 (a) and (b)

Uneven and cracked surface can be seen in the untreated samples which may be due to the presence of impurities in the fibre. The micrograph depicts the crystalline nature. This shows the typical micrograph of the clustering of well established randomly oriented nano rods which has compact, homogenous and well adherent growth onto the substrate.

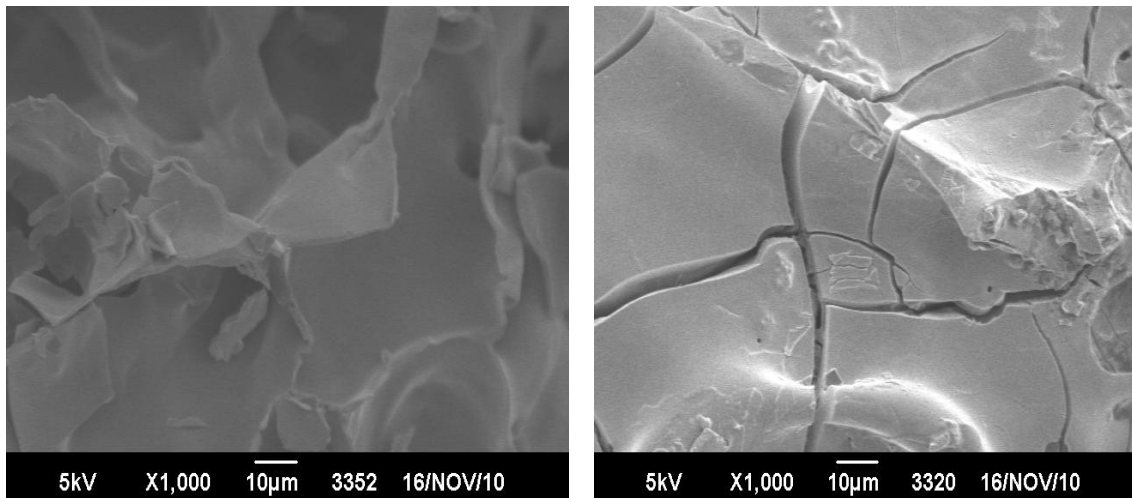


Fig 6 (a) and (b)

There was change in the unevenness of the surface in contrast of treated fibre it may be due to the chemical treatment done on the fibre. All images show the morphology of material and fiber respectively. Figures have porosity, non uniform and inside hollow texture. Its upper surface is in crystalline, non linear, soft and spongy form. These figures fiber shows a crystalline, linear and smoky effect.

#### TEM

Fig 7 (a) (b) and (c) for SP1, SP2 & SP3 respectively shows the non linear and non uniform dispersed aluminum oxide particles of 110.57nm and the agglomerated fiber containing 284.63-156.92nm size particles of aluminum oxide. The samples appear highly strained as seen in fig 7 (a) (b) and (c). The presence of dislocation loops is clearly seen. It is possible that the strain present in the sintered samples has a direct effect on the dielectric loss. The TEM micrographs show the heterogeneous microstructure aluminum oxides. A heterogeneous distribution of the individual phases is observed in all heterogeneous systems. On the other hand, in the aluminum oxide samples the particles possess needles like morphology with non-uniform sizes in a range from 110.57nm to 284.63-156.92nm.

These needles are less in numbers but large in size. The TEM investigations of the aluminum oxide composite samples show heterogeneous distribution with aluminum oxide needle like structure of about 30nm sizes. The diffraction pattern shows a higher grade of crystalline for the high aluminum oxide containing sample. The first fig shows the magnification 40000 which shows total palate of size of 110.57nm, second fig shows with the magnification of 60000 which is clearly shows the fibrous portion of the palate 284.63nm and third fig shows the magnification of 12000 which again shows the fibrous portion of the palate 156.92nm.

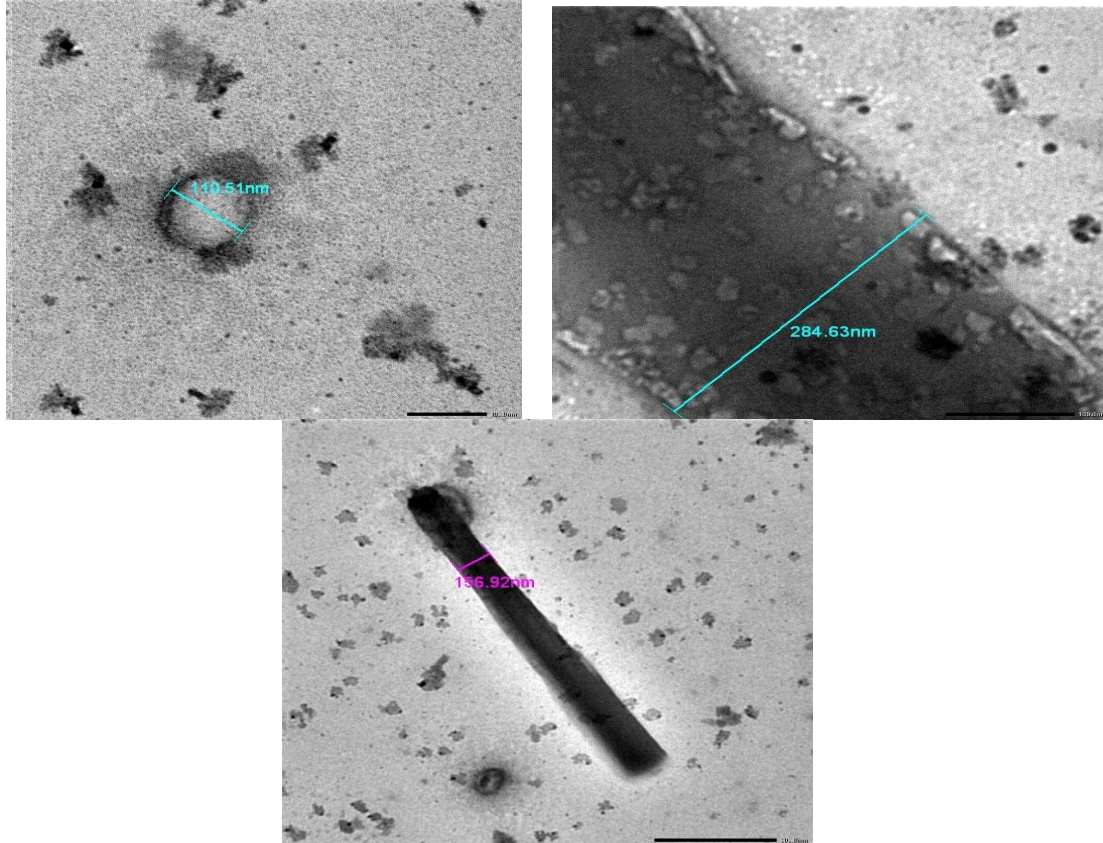


Fig (c)

Fig74. (a) (b) and (c) TEM of  $\text{Al}_2\text{O}_3$  to find the structure and composition of the sample prepared in our studies. The TEM graphs show the highly homogeneous microstructure if  $\text{Al}_2\text{O}_3$  samples the aluminum nitrate and ammonium chloride (10:4) one has still amorphous particles. The TEM investigations of the  $\text{Al}_2\text{O}_3$  composite samples show heterogeneous distribution with needle like structure. Among the sisal fiber doped aluminum samples with the composition has a longer amount of pores in the microspores region. Hence the pores size can be adjusted by the composition according to needs of the applications TEM observations confirmed the homogeneity of the microstructure. The morphology of the composites consists of aluminum oxide needles with high aspect ratio. It is possible to synthesize materials with different porosity features and surface morphology, which result in different applications by changing the ration of individual components in oxide system [28].

#### FTIR

The formation of  $\alpha\text{-Al}_2\text{O}_3$  was approved by FTIR spectrum in figures showed that  $\alpha\text{-Al}_2\text{O}_3$  is known to have spinal structures which exist over a range of hydrogen content captured by the empirical formula  $\text{H}_{3m}\text{Al}_{2-m}\text{O}_3$ . It is clear that broad absorption bands appear at  $3500\text{-}500\text{cm}^{-1}$  respectively, which is attributed to the stretching vibration of hydroxyl groups. The peaks at  $3127.07$ ,  $1399.42$  and  $584.57\text{ cm}^{-1}$  correspond to the vibration of carboxylic acid groups. The IR transmission spectra of sisal fiber composite shown in fig from fig 8, 9 & 10 for SP1, SP2 & SP3 respectively were recorded in the range  $3700\text{-}3400\text{ cm}^{-1}$ . The wave number of fig 8 (SP1)  $3127.0691$ ,  $2358.4974$ ,  $1641.0773$ ,  $1399.4211$  and  $584.5742\text{cm}^{-1}$  shows the width  $1471.2957$ ,  $1716.5060$ ,  $82.7603$ ,  $40.8444$  and  $378.2537\text{cm}^{-1}$  of IR spectra respectively.

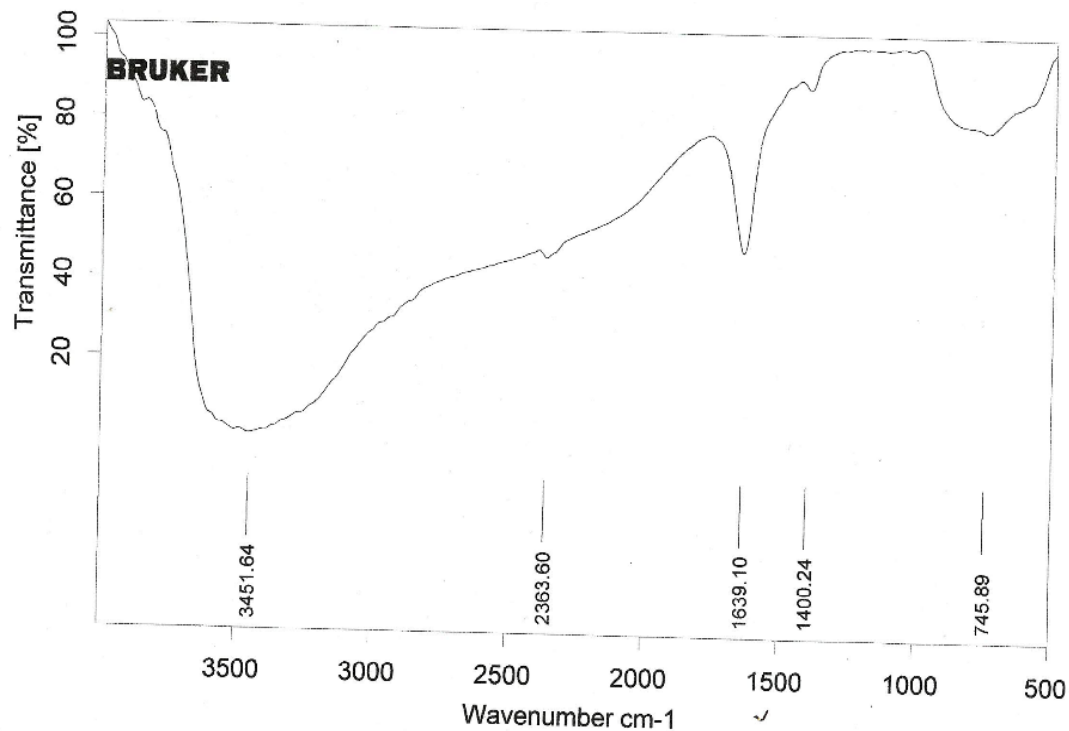


Fig. 8 Intensity of Transmittance versus wave number (courtesy SIRT-F Bhopal)

The prepared sample was free from visible inhomogeneities like cracks or bubbles. Decrease with a shifting of meta-center towards slightly higher wave number. For further increase of  $\text{Al}_2\text{O}_3$  the intensity of this band is continued to decrease where the first group of bands is also observed to decrease [29]. The peaks at 3447.86, 1639.35 and 586.54  $\text{cm}^{-1}$  correspond to the vibration of carboxylic acid group. The wave number of fig 9 (SP2) 3447.86, 2360.13, 2072.60, 1639.35, 1397.30, 642.20 and 586.54  $\text{cm}^{-1}$  shows the width 445.6188, 60.6905, 203.3672, 82.8672, 44.0294, 92.4690 and 294.6694  $\text{cm}^{-1}$  of IR spectra respectively.

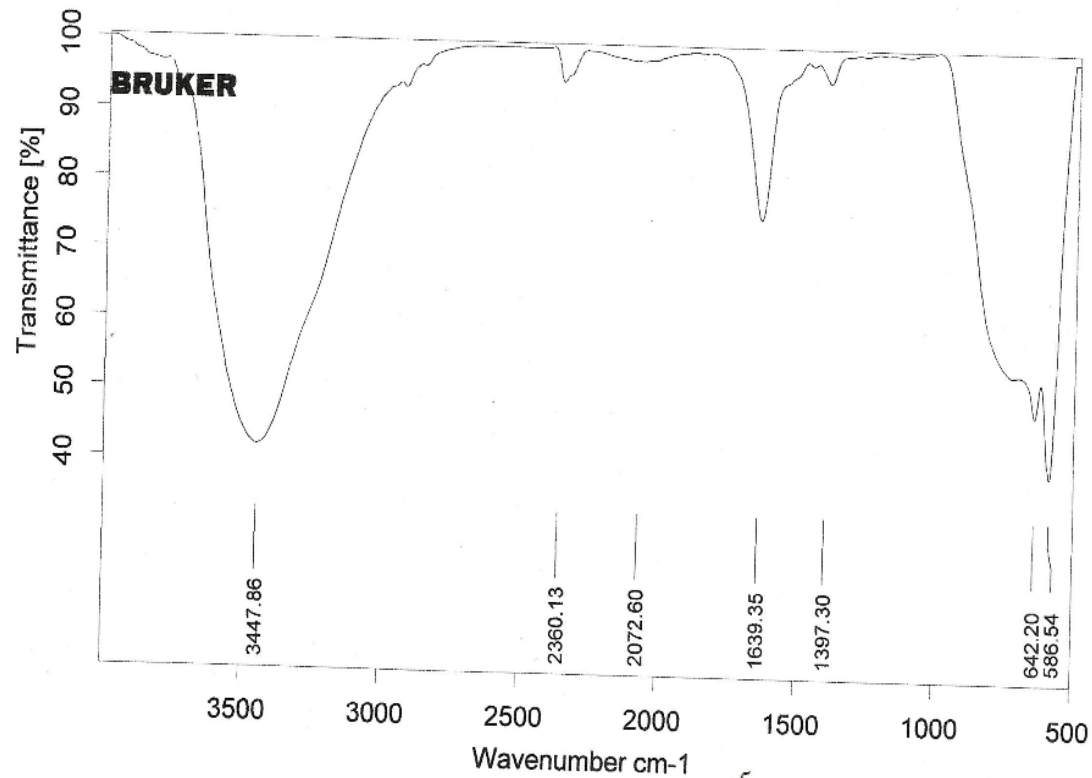


Fig. 9 Intensity of Transmittance versus wave number another sample (courtesy SIRT-F Bhopal).

The peaks at 3450.73, 1638.44 and 589.85  $\text{cm}^{-1}$  correspond to the vibration of carboxylic acid group. The wave number of fig 10 (SP3) 3450.73, 2360.94, 1638.44, 740.04 and 589.85  $\text{cm}^{-1}$  shows the width 558.7216, 54.5087, 79.0997, 366.1014 and 46694.4103  $\text{cm}^{-1}$  of IR spectra respectively. The prepared sample was free from visible inhomogeneities like cracks or bubbles. Decrease with a shifting of meta-center towards slightly higher wave number. For further increase of  $\text{Al}_2\text{O}_3$  the intensity of this band is continued to decrease where the first group of bands is also observed to decrease [29].

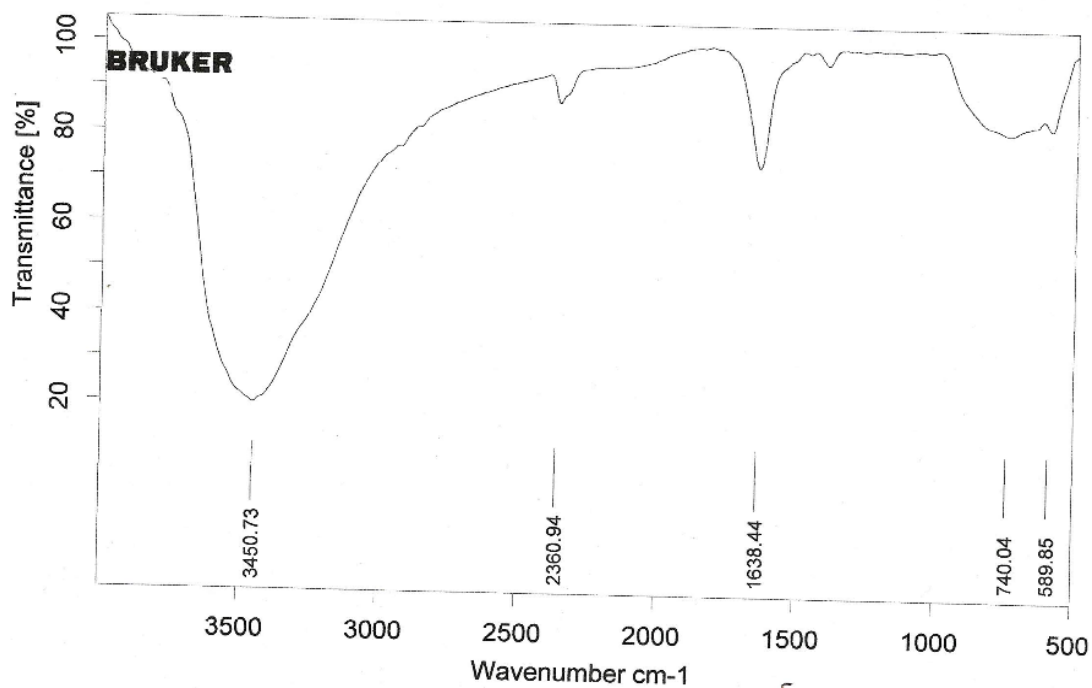


Fig.10 has several valleys imitating influence of dopants. The prominent valley at  $3437\text{ cm}^{-1}$  is interesting (courtesy SIRT-F Bhopal).

The stronger broadening bands  $3500\text{-}1000\text{ cm}^{-1}$  for SP1,  $3400\text{-}900\text{ cm}^{-1}$  for SP2 and  $3300\text{-}800\text{ cm}^{-1}$  for SP3 occurs due to the hydrogen bond between the various hydroxyl groups in the product. The stronger broadening bands  $3700\text{-}3400\text{ cm}^{-1}$  for SP1, SP2 & SP3 correspond to Al-O vibration existed under the temperature of  $1000^\circ\text{C}$  at 15, 30 and 45 min for SP1, SP2 and SP3 respectively. In agreement with other works it is resulted that the main factor in obtaining of different aluminum oxide phases is the calcinations temperature at  $1000^\circ\text{C}$  leads to form the  $\alpha\text{-Al}_2\text{O}_3$  [30].

#### Dielectric behavior

The electrical properties of the insulating material  $\text{Al}_2\text{O}_3$  composite were measured by impedance analyzer these dielectric measurement of  $\text{Al}_2\text{O}_3$  composite doped with sisal fiber shown in fig 11 and 12. In the Fig 11 represents the graph between frequency and  $\tan\delta$  and fig 12 shows the comparison between frequency and  $\epsilon$ .

The dielectric constant  $\epsilon$  and loss  $\tan\delta$  of  $\text{Al}_2\text{O}_3$  at room temperature  $30^\circ\text{C}$  are measured to be 1.9 to 1.3 respectively and are found to decrease with the increase in the frequency. The value of  $\epsilon$  and  $\tan\delta$  are found to different with each other. In fig 11 the variation of dielectric constant at different frequencies with room temperature  $30^\circ\text{C}$  for  $\text{Al}_2\text{O}_3$  is shows that it decreases considerably with increase in frequency.

This dielectric dispersion is attributed to the Maxwell and Wagner type of interfacial polarization in agreement with Koop's phenomenological theory [31]. Since polarization decreases with increasing frequency and reaches constant values, a decrease in dielectric constant with frequency is observed.

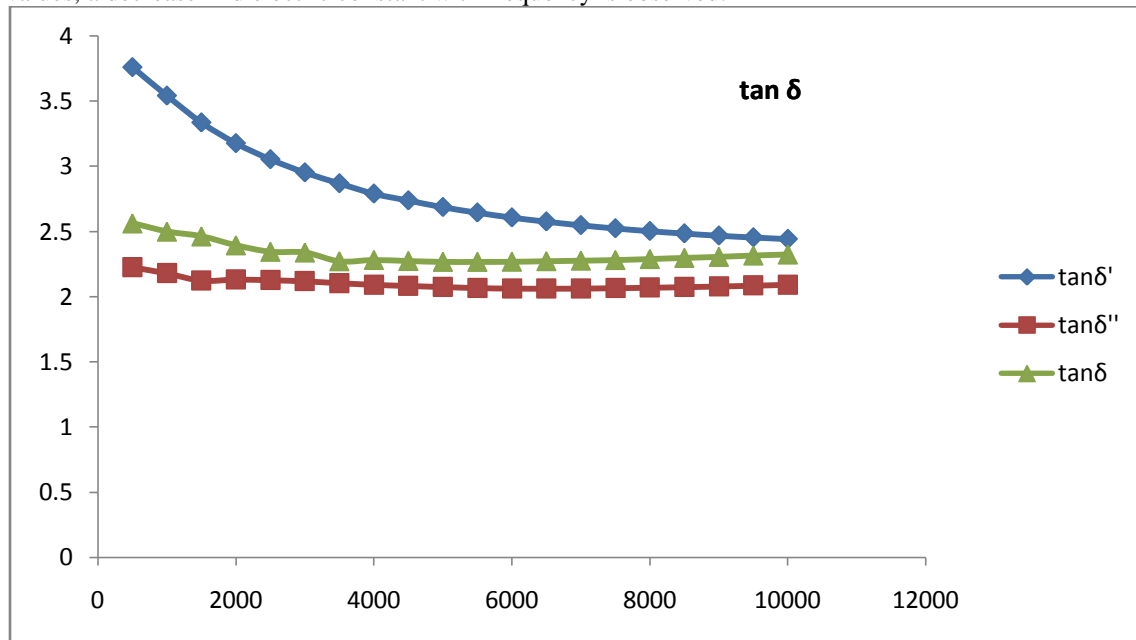


Fig 1

At lower frequencies, dielectric loss  $\tan\delta$  is large and it decreases with increasing frequency. The  $\tan\delta$  is the energy dissipation in the dielectric system, which is proportional to the imaginary part of the dielectric constant. An increase in loss factor at higher frequencies may be due to the series resistance of the electrodes, leads, etc [32-34].

While in fig 12 is a comparison plot of variation of dielectric constant with different frequency at constant temperature shows an increase considerably with increase in frequency. It was observed from these figures that the dielectric constant increases continuously with increase in frequency for all the samples, followed with a frequency independent behavior.

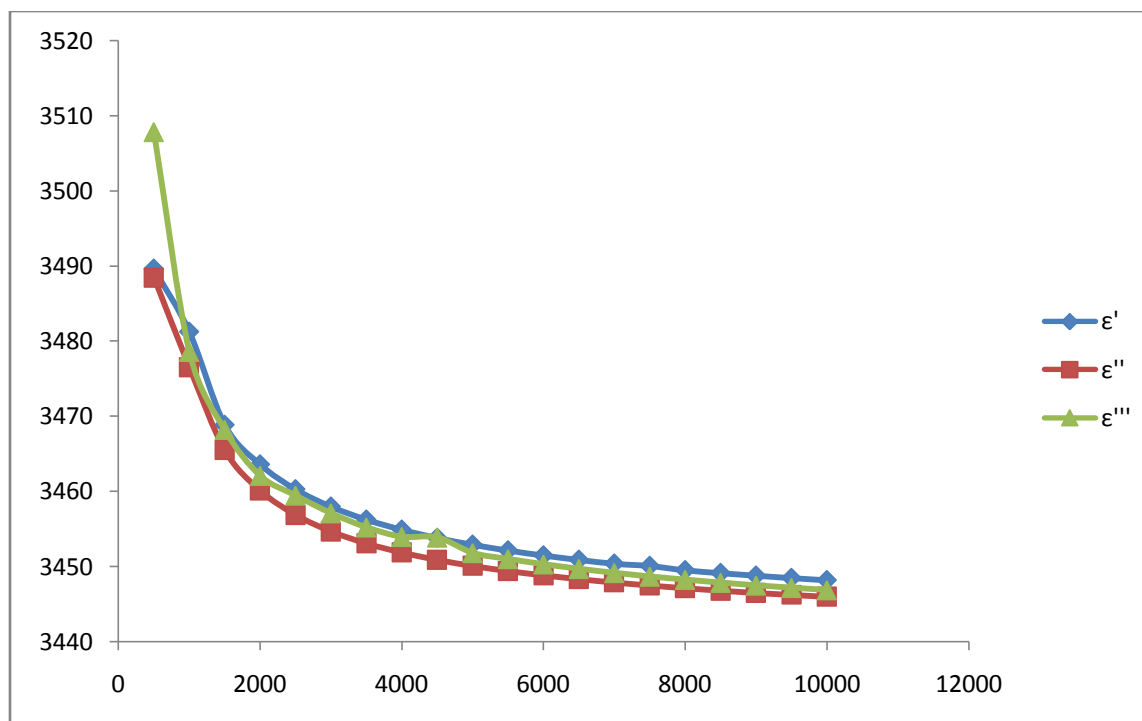


Fig 12

The dielectric properties of Alumina are dependent upon several factors, including the method of preparation, chemical composition and grain structure, size and natural fiber (sisal fiber) and it's contains cellulose, hemicelluloses, lignin and pectin. The observed dielectric behavior of our samples may also be due to the particle size effect and is also in concurrence with observation made by other Investigators [35, 36]. The effect of electrical homogeneity fine grain structure and shape of the Alumina samples affect the dielectric properties [37]. It also presence the  $\alpha$  impurities contributes towards the change in dielectric properties. The dielectric constant of 25-30 at 10 KHz and an increasing trend is observed at higher frequencies. This is normal behavior for high density fine chemically homogenous material [38].

The electronic exchange between Ammonium and aluminum ions didn't follow the path of frequency which is externally applied alternating beyond the critical frequency value. The dielectric behavior of samples shown in graphs is because of its particle size effect [39]. If  $\epsilon$  remains unaffected with increase in temperature then frequency also remains the same, which means that the local carriers are immobile. It is understood that the local charge carriers are immobile and the thermal activation is negligible. This further suggests that the samples possess a high chemical homogeneity and fine grain distribution. The presence of moisture, cellulose, hemicelluloses, lignin and pectin is also indicated by the electrical conductivity results. It is reported the presence of moisture plays an important role in the formation and stabilization of  $\text{Al}_2\text{O}_3$  [40].

## Conclusion

From the above study it is clear that chemical treatment of sisal fibre is an effective method to modify the properties of fibre. Change in the morphology of sisal fibre has been seen through SEM analysis. An XRD study reveals the crystal structure of the samples. The effect of chemical homogeneity, fine structure, particle size and shape of the aluminum samples are understood to affect the properties of its dielectric properties, TEM and FTIR behavior. The presence of moisture, cellulose, hemicelluloses, lignin and pectin also contribute towards changes in composites properties. In this agreement with other works, it is resulted that the main factor in obtaining of alumina is the calcinations temperature on different time durations. The presence of moisture, cellulose, hemicelluloses, lignin and pectin also contribute towards changes in dielectric properties.

## References

1. Burkat, V.S.; Dudorova, V.S.; Smola, V.S.; Chagina, T.S. *Light Metals* 1985, 1443.
2. Nedez, C.; Boitiaux, J.-P.; Cameron, C.J.; Didillon, B. *Langmuir* 1996, 12, 3927.
3. Okada, K.; Tanaka, A.; Hayashi, S.; Daimon, K.; Otsuka, N. *J. Mater.* 1994, 9, 1709.
4. Ananthakumar, S.; Raja, V.; Warriar, K.G.K. *Mater. Lett.* 2000, 43, 174.
5. Chen, Y.; Jin, L.; Xie, Y.J. *Sol-Gel Sci. Technol.* 1998, 13, 735.
6. Xue, D.S.; Huang, Y.L.; Ma, Y.; Zhou, P.H.; Niu, Z.P.; Li, F.S.; Job, R.; Fahrner, W.R.J. *Mater. Sci. Lett.* 2003, 22, 1817.
7. Yang, A.; Tao, X.M.; Pang, G.K.H.; Siu, K.G.G. *J. Am. Ceram. Soc.* 2008, 91(1), 257.
8. Panda, P.K.; Ramakrishna, S.J. *Mater. Sci.* 2007, 42(6), 2189.
9. Kar, S.; Chaudhuri, S.J. *Phys. Chem. B* 2006, 110(10), 4542.
10. Huyn, W.U.; Dittmer, J.J.; Alivisatos, A.P. *Science* 2002, 295, 2425.
11. Duan, X.; Huang, Y.; Agarwal, R.; Lieber, C.M. *Nature* 2003, 421, 241.
12. Li, L.S.; Walda, J.; Manna, L.; Alivisatos, A.P. *Nano Lett.* 2002, 2, 557.
13. I.V. Cutler, C. Bradshaw, C.J. Christensen and E.P. Hyatt, *J. Amer. Ceram. Soc.*, 40(1957) 134-139.
14. W.C. Johnson and R.L. Coble, *J. Amer. Ceram. Soc.* 61(1978) 110-114.
15. D.R. Merrill, M. Bikson and J.G.R. Jeffreys, *J. Neuroscience Methods*, 141(2005) 171-198.
16. H. Erkalfa, Z. Misirli and T. Baykara, *Ceramics International* 21(1995) 345.
17. A.R. Boccaccini and C. Kaya, *Ceramics International* 28(2002) 893-897.
18. M. Sathiyakumar and F.D. Gnanam, *Ceramics International* 28(2002) 195.
19. F.-S. Shiau and T.-T. Fang, *Mater. Chem. and Phys.* 60(1999) 91-94.
20. L.C. Pathak, T.B. Singh, S. Das, A.K. Verma and P. Ramachandrarao, *Mater. Lett.* 57(2002) 380.
21. P.V. Ananthapadmanabhan, T.K. Thiyagarajan, K.P. Sreekumar and N. Venkatramani, *Scripta Mater.* 50(2004) 143-147.
22. J.H. Park, M.K. Lee, C.K. Rhee and W.W. Kim, *Mater. Sci. and Eng. A*, 375-377 (2004) 1263-1268.
23. G.R. Karagedov and N.Z. Lyakhov, *Nanostructured Materials* 11(1999) 559-572.
24. s.k. dhawan kuldeep singh, anil, a.k. bakhshi polymeric & soft materials section. National physical laboratory. New delhi-110021. India
25. ek et al. 1989
26. Schmittle, M.; Burghart, A. *Angew. Chem. int. Ed. EEngl.* 1997, 36, 2550.
27. Phase Transformations of  $\alpha$ -Alumina Made from Waste Aluminum via a Precipitation Technique Khamirul Amin Matori, Loy Chee Wah, Mansor Hashim, Ismayadi Ismail and Mohd Hafiz Mohd Zaid *Int. J. Mol. Sci.* **2012**, 13(12), 16812-16821; doi:[10.3390/ijms131216812](https://doi.org/10.3390/ijms131216812)
28. W. Wunderlich, P. Padmaja, K.G.K. Warriar TEM characterization of sol-gel-processed alumina-silica and alumina-titania nano-hybrid oxide catalysts *Journal of the European Ceramic Society* 24 (2004) 313-317
29. S yusub, Gsahaya baskaran et al *Indian journal of pure & applied physics* Vol. 49 May 2011. Pp 315-322.

30. Seyed Ali Hosseini, Aligholi Niaei, Dariush Salari Production of  $\gamma$ -Al<sub>2</sub>O<sub>3</sub> from Kaolin Open Journal of Physical Chemistry, 2011, 1, 23-27 doi:10.4236/ojpc.2011.12004 Published Online August 2011
31. Maxwell J C. Electricity and magnetism. London: Oxford University Press, 1993: 828
32. Sawant V S, Shinde S S, Deokate R J, et al. Effect of calcining temperature on electrical and dielectric properties of cadmium stannate. Appl Surf Sci, 2009, 255: 6675
33. Babar A R, Shinde S S, Moholkar A V, et al. Electrical and dielectric properties of co-precipitated nanocrystalline tin oxide. J Alloys Compd, 2010, 505: 743
34. Goswami A, Goswami A P. Dielectric and optical properties of ZnS films. Thin Solid Films, 1973, 16: 175
35. J. Volger, Philips tech. Rdsch. 22, 306 (1960/61)
36. Das and Pramanik 1998; Rane et al 2001
37. Murthy 1990
38. Katsumi et al 1975
39. Vijaya Hiremath and A Venkataraman 2002
40. Rehman and Venkataraman 2002